

Preparation and evaluation of 2-azinyl-2*H*-benzotriazoles as bidentate ligands: Synthesis and characterization of [2-(2-pyridinyl)-2*H*-benzotriazole](*bpy*)₂Ru²⁺

Emilia Obijalska^{a,b,1}, Piotr Kaszynski^{a,b,*}, Aleksandra Jankowiak^a, Victor G. Young^c

^a Organic Materials Research Group, Department of Chemistry, Vanderbilt University, Nashville, TN 37235, USA

^b Faculty of Chemistry, University of Lodz, Tamka 12, 91-403 Łódź, Poland

^c Crystallographic Laboratory, Department of Chemistry, University of Minnesota, Twin Cities, MN 55455, USA

ARTICLE INFO

Article history:

Received 6 November 2010

Accepted 15 February 2011

Available online 19 February 2011

Keywords:

Heterocycle

Ligand

Synthesis

Ru complex

DFT calculations

ABSTRACT

Five 2-azinyl-2*H*-benzotriazoles (azinyl = 2-pyridinyl, 2-pyrazinyl, 2-pyrimidinyl, 6-methoxy-3-pyridazinyl, 5-methyl-2-pyridinyl) were prepared and characterized as bidentate ligands. The electronic structure of these and related heterocycles was investigated spectroscopically and computationally (TD-DFT). They were tested at the B3LYP/6-31++G(d, p)//B3LYP/6-31G(d, p) level of theory as ligands for MgH₂, which permitted the elucidation of trends in complex formation, its geometry as a function of the ring structure, and the number and position of the nitrogen atoms in the azine ring. A Ru²⁺ complex **7a-Ru** with 2-pyridinyl-2*H*-benzotriazole (**7a**) and two *bpy* ligands was prepared and characterized structurally, spectroscopically and electrochemically. The results were compared to those for similar complexes and discussed in the context of computational results for MgH₂ complexes.

© 2011 Elsevier Ltd. All rights reserved.

1. Introduction

Heteroaromatic bidentate ligands are important chelates that tune photophysical and electrochemical properties of transition metal complexes. Perhaps the best known and most extensively studied such a ligand is 2,2'-bipyridyl (**1**), whose ruthenium complexes [1,2] **1-Ru** have been explored as components of energy harvesting [3,4] and electroluminescence [5] devices. Replacement of one of the pyridine rings in **1** with fused five-membered heterocycle, such as indole [6,7] or benzimidazole [8,9] in **2** and **3** respectively, leads to anionic ligands and complexes with reduced overall charge. Recently, there has been interest in electrically neutral bidentate ligands based on the fused azole-pyridine structural motif. Such ligands offer different geometry of the coordination site and additional means of controlling red-ox and photophysical properties of the metal complexes [10,11]. Examples of such ligands are **4**, **5**, and **6** and their complexes **4-M**–**6-M** [12–14]. These and other nitrogen-rich ligands [15,16] are of interest for designing dinuclear complexes [8,17,18] and controlling their supramolecular structures [19–21] and functions [2].

All three ligands **4**–**6** are based on fused triazole substituted with pyridine, and they differ significantly in their electronic structures. In contrast to **4**, derivatives **5** and **6** have a quinoid structure

in their non-polar ground states and lower HOMO–LUMO gaps. A similar quinoid structure exists for 2-pyridinyl-2*H*-benzotriazole (**7a**), an isomer of **4**, but surprisingly, neither **7a** nor its close analogs have been investigated to date.

Here we focus on pyridine derivative **7a** and its polyazine analogs **7b**–**7e** as new potential bidentate ligands for transition metals. The new ligands are evaluated for their photophysical properties and chelating ability of MgH₂ using DFT computational methods. We described the preparation and spectroscopic analysis of the parent ligands **7a**–**7c** and two of their derivatives, **8** and **9**. Finally, a ruthenium complex **7a-Ru** was prepared and analyzed structurally, spectroscopically, and electrochemically. The experimental data were compared to the computational results.

2. Results and discussion

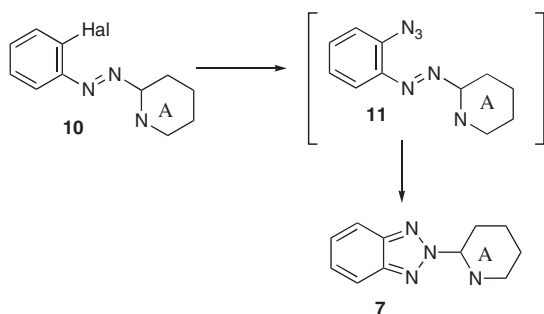
2.1. Synthesis

The triazoles **7** were prepared from appropriate haloazo derivatives **10** according to a modified general method [22] for substituted 2-phenylnaphtho[1,2,3]triazoles (Scheme 1). Thus, a reaction of chloro derivative **10a** (Hal = Cl) with excess NaN₃ in DMF at 120 °C gave 32% yield of **7a**. Addition of catalytic amounts of [Bu₄N]⁺Br[−] improved the yield to 49%. Replacement of the chlorine by fluorine in **10a** (Hal = F) increased the yield of **7a** further to 79%, which is attributed to a more facile nucleophilic displacement of the F[−] than Cl[−] in azobenzenes [23]. Attempts to isolate the transient azide **11** by running the reaction in boiling MeCN were

* Corresponding author. Tel.: +1 615 322 3458; fax: +1 615 343 1234.

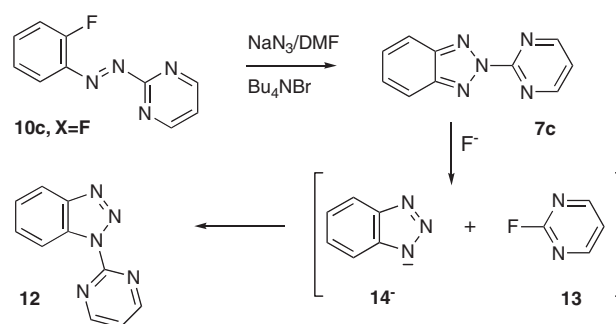
E-mail address: piotr.kaszynski@vanderbilt.edu (P. Kaszynski).

¹ A visiting student from the laboratory of Professor Grzegorz Mloston, University of Łódź, Poland.



Scheme 1.

unsuccessful and only starting material **10a** was fully recovered after 60 h. The higher efficiency of the reaction of the fluorides than chlorides, prompted us to use fluorides **10b** and **10c** (Hal = F) for the preparation of the corresponding triazoles **7b** and **7c**.

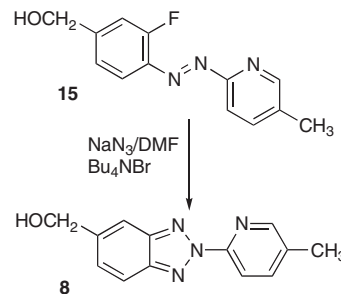


Scheme 2.

(6.3 kcal/mol in gas phase). To eliminate nucleophilic halide ions, the reaction was conducted with 4 equiv. of NaN₃ in the presence of small excess of Ca(OTs)₂ as the fluoride ion scavenger, and [Bu₄N]⁺Br⁻ was replaced with [Bu₄N]⁺[HSO₄]⁻. The reaction gave a mixture (28% yield) of **7c** and **12** in 1:2 ratio and benzotriazolone (**14**) isolated in 56% yield. To avoid the presence of nucleophiles such as traces of water or Me₂NH from decomposing DMF, the reaction was run in freshly dried MeCONMe₂ (DMA) with stoichiometric amounts of rigorously dried NaN₃ and Ca(OTs)₂. The isolated yield of **7c** was little affected by these precautions, and the approximate ratio of the products **7c**:**12**:**14** was 3:2:2 in one run and 2:5:3 in another by ¹H NMR. The desired 2-isomer was isolated as the least polar fraction that on TLC appears as a fluorescent spot. Results for **7c** suggest that the preparation of the triazine derivative **7e** by this method may be even more challenging considering the electrophilic nature of the C(2) atom in the triazine ring.

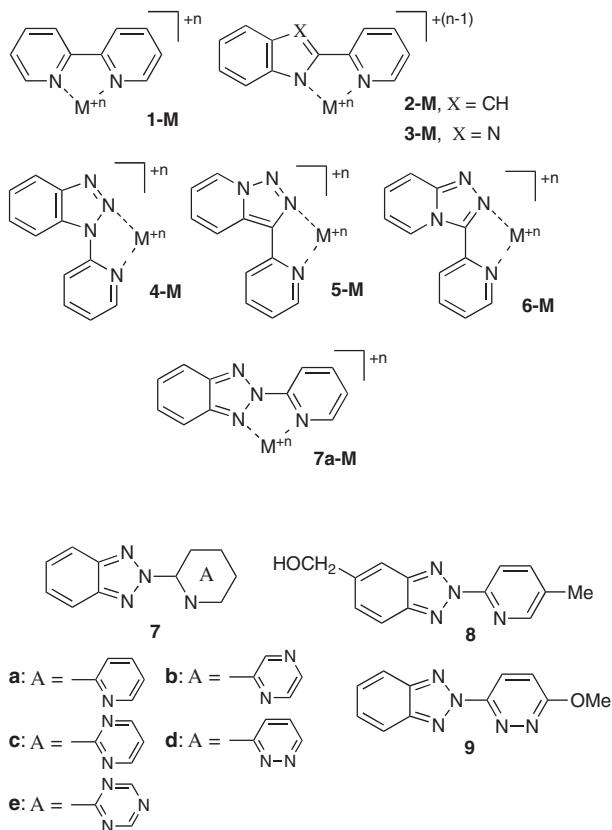
Finally, we prepared substituted derivatives, pyridine **8** (Scheme 3) and pyridazine **9** (Scheme 4), using appropriately functionalized azo compounds **15** and **16**, respectively. In the case of pyridazine **9**, the major product (51% yield) was the more polar isomeric compound **17**, which was identified on the basis of NMR and IR data. The origin of the formation of **17** is unclear although similar *O*- to *N*-rearrangements were observed before at elevated temperatures for other alkoxy pyridazines [26]. Heating of product **9** with or without [Bu₄N]⁺Br⁻ in DMF did not give the rearrangement to **17**. In contrast, substrate **16** heated with catalytic amounts of [Bu₄N]⁺Br⁻ gave 21% of the rearranged product identified as **18** on the basis of the ¹H NMR spectrum and appearance of a signal at 3.97 ppm at the expense of the characteristic signal for the OMe group at 4.25 ppm. A reaction of **16** and NaN₃ conducted without [Bu₄N]⁺Br⁻ gave 8% yield of the expected isomer **9** and 24% yield of the rearranged product **17**.

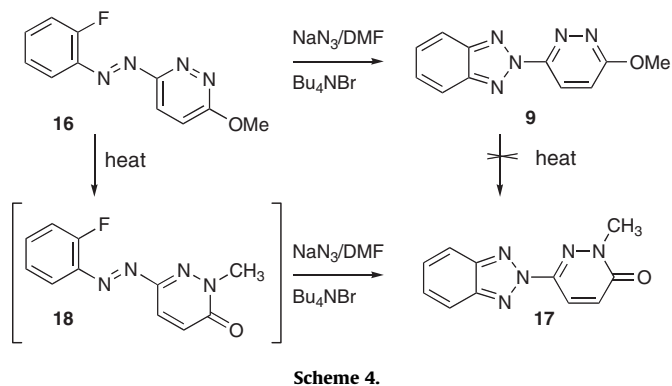
The azo derivatives **10** and **16** were obtained using the general procedure [27] by condensing either 2-chloro- or 2-fluoronitrosobenzene with appropriate aminoazine in aq 50% NaOH/toluene system. The details of the preparation of **10a** and **15** will be described elsewhere [28].



Scheme 3.

A reaction with azopyrazine **10b** gave the expected triazole **7b** in a good yield. In contrast, a reaction of the pyrimidine derivative **7c** under the same conditions gave exclusively the known [24] 1-isomer **12**, which was isolated in 56% and identified by comparison of the NMR, UV and IR spectra with the literature data [25]. We speculated that the fluoride anion formed in the reaction attacks the electrophilic C(2) position of the pyrimidine ring (Scheme 2), which results in the formation of electrophilic 2-fluoropyrimidine **13** and benzotriazolone ion (**14**⁻). Subsequent nucleophilic aromatic substitution of fluoride in **13** with the anion **14**⁻ led to **12**. Arylation of benzotriazolone (**14**) with 2-bromo-[24] or 2-chloropyrimidine [25] was reported to give **12** as the only isolated product. Calculations at the B3LYP/6-311G(d,p) level of theory confirmed that the 1-isomer **12** is more thermodynamically stable than the desired 2-isomer **7c** by 5.7 kcal/mol in MeCN dielectric medium





2.2. Electronic absorption and emission spectra

Experimental absorption and emission spectra for triazoles **7a–7c**, **9**, **12**, and **17** were recorded in MeCN, and the results are presented in Figs. 1–3 and Table 1. All four 2-substituted benzotriazoles exhibit a strong absorption band at about 305 nm and a weaker band around 228 nm, as shown for **7a** in Fig. 1. This is consistent with results for other simple 2-aryl-2H-benzotriazoles such as **19** (Table 1) [29,30].

Absorption spectra for 1-substituted benzotriazoles are different from those of the 2-isomers. For instance, the absorption band at about 300 nm recorded for **7c** has significantly reduced intensity and is slightly blue-shifted in its 1-isomer **12** (Fig. 2). There are smaller albeit noticeable differences in the absorption spectra of the two isomeric pyridazines (Fig. 3). The *N*-Me isomer **17** has a broader absorption band around 300 nm than its *O*-Me isomer **9** containing the aromatic pyridazine ring.

Three of the new triazoles **7a**, **7b**, and **7c** fluoresce. The pyridine derivative **7a** exhibits the most efficient photoluminescence with a maximum at 364 nm. For the pyrazine and pyrimidine derivatives **7b** and **7c** the emission energy is lower by 0.18 and 0.12 eV, respectively, and the emission efficiency is about 20% and 10%, respectively, relative to that observed for **7a** (Table 1). In contrast, triazole **12**, an isomer of **7c**, and the two pyridazines **9** and **17**, do not exhibit a detectable fluorescence at ambient temperature.

Absorption spectra were calculated using the TD-DFT method for structures optimized at the B3LYP/6-311G(d, p) level of theory. The heterocycles were found in the C_s symmetry (**4** [31], **5**, **6**, **7a**, **7b**, **7d**, and **9**), C_{2h} (**1**) [32], C_2 (**7c**) [33], and C_{2v} (**7e** and **19**) [34],

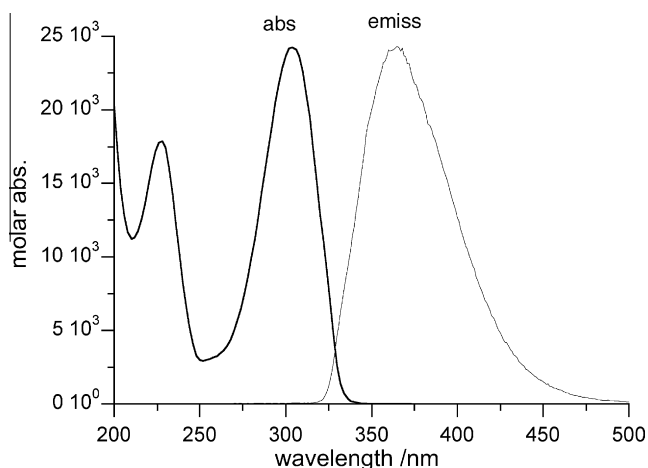


Fig. 1. Electronic absorption (bold line) and emission spectra of **7a** recorded in MeCN. The emission spectrum in arbitrary units.

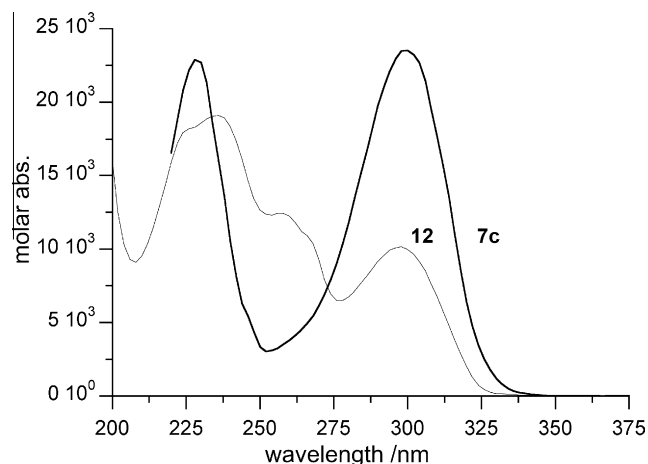


Fig. 2. Electronic absorption spectra of **7c** (bold line) and **12** recorded in MeCN.

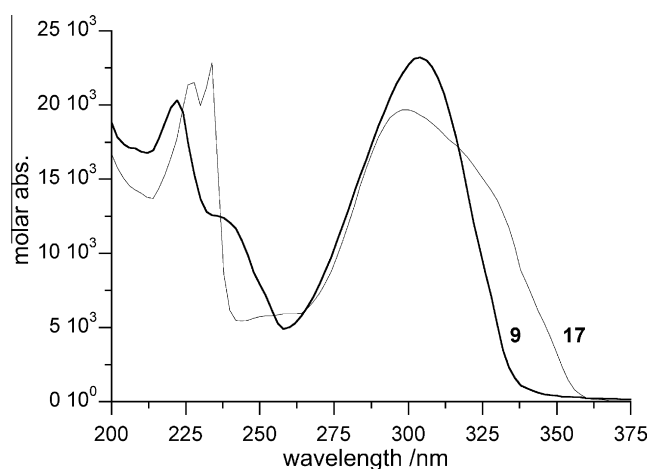


Fig. 3. Electronic absorption spectra of **9** (bold line) and **17** recorded in MeCN.

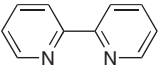
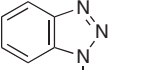
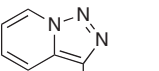
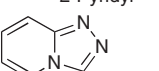
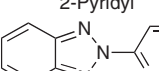
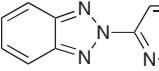
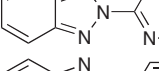
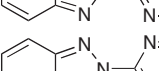
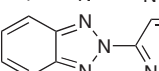
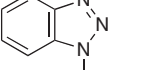
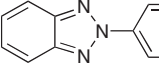
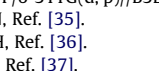
which is consistent with their reported experimental solid-state structures.

Computational results demonstrated that the intense low energy absorption bands for 2-substituted benzotriazoles **7** are located around 300 nm, which is in good agreement with the available experimental data (Table 1). The main component of this π - π^* excitation typically is the HOMO – 1 \rightarrow LUMO transition with a small contribution from the HOMO \rightarrow LUMO + 1 transition. The former set of MOs extends over the entire π system, while the MOs involved in the latter transition are localized as shown for **7a** in Fig. 4. The exception is the pyridazine **7d** for which the HOMO-1 contains the lone pairs of the pyridazine ring and the π orbital participating in the π - π^* excitation is the HOMO – 2.

The transition energy of the 2-substituted benzotriazole is affected by the number and the position of the nitrogen atoms in the azine ring. Upon substitution of the pyridine ring in **7a** for phenyl in **19** the π - π^* excitation energy increases by 7 nm (experimental 4 nm) and by an additional 9 nm (experimental 4 nm) in pyrimidine, pyridazine and triazine derivatives. Only in the pyrazine derivative **7b** the transition energy decreases markedly. This trend approximately follows the trend in energy of the LUMO in the series from the highest in the phenyl derivative **19** (–2.02 eV) to the lowest in the triazine **7e** (–2.69 eV).

A comparison of the results for 2-pyridinyl and 1-pyridinyl derivatives **7a** and **4**, respectively, shows the same type of delocalized MOs (HOMO and LUMO) involved in the π - π^* transitions and

Table 1
Experimental and calculated absorption energies and oscillator strength for selected ligands.

Ligand	Symm	LUMO/eV	Experimental		Theoretical ^a $\pi \rightarrow \pi^*/\text{nm}$ (<i>f</i>)	
			Absorption (nm (log ϵ))	Emission (nm)	Vacuum $\epsilon = 1$	MeCN $\epsilon = 35.7$
1 	C _{2h}	-1.59	283 (4.16) ^b 284 ^d	365 ^c	267 (0.46)	272 (0.57)
4 	C _s	-1.75	^e	^e	292 (0.27)	298 (0.32)
5 2-Pyridyl 	C _s	-1.68	317 (4.16) ^f 305 (4.18) ^f	412 ^g	334 (0.20) 289 (0.18)	327 (0.35) 288 (0.14)
6 2-Pyridyl 	C _s	-1.61	^e	^e	311 (0.19) 305 (0.26)	311 (0.44) 300 (0.14)
7a 	C _s	-2.12	304 (4.38) ^h	364 ^h	291 (0.59)	299 (0.73)
7b 	C _s	-2.42	311 (4.39) ^h	384 ^h	296 (0.48) 280 (0.17)	303 (0.70)
7c 	C ₂	-2.24	299 (4.37) ^h	377 ^h	282 (0.62)	290 (0.67) 276 (0.12)
7d 	C _s	-2.37	^e	^e	282 (0.59)	295 (0.31) 286 (0.46)
7e 	C _{2v}	-2.69	^e	^e	282 (0.55)	293 (0.47) 284 (0.27)
9 	C _s	-2.17	304 (4.36) ^h	^{h,i}	298 (0.42) 287 (0.24)	305 (0.71) 283 (0.10)
12 	C _s	-1.87	298 (4.00) ^h 300 (4.08) ^j	^{h,i}	289 (0.17)	294 (0.31)
19 	C _{2v}	-2.02	308 (4.38) ^k	368 ^k	298 (0.62)	306 (0.75)

^a TD-B3LYP/6-311G(d,p)//B3LYP/6-311G(d,p).

^b In MeCN, Ref. [35].

^c In MeOH, Ref. [36].

^d In EtOH, Ref. [37].

^e Not reported.

^f In MeOH, Ref. [31].

^g Ref. [38].

^h In MeCN; this work.

ⁱ Not detected.

^j In EtOH, Ref. [22].

^k In MeOH, Ref. [30].

little difference in the electronic excitation energy. In the isomeric [1,2,3]triazolo[1,5-*a*]pyridine derivative **5** and [1,2,4]triazolo[4,3-*a*]pyridine **6**, there are two $\pi-\pi^*$ excitations that are generally lower energy than those calculated for **7a** and **4** (Table 1), which result mainly from the HOMO \rightarrow LUMO (low energy) and HOMO \rightarrow LUMO + 1 (high energy) transitions.

The inclusion of the PCM solvation model showed a modest positive solvatochromic effect on the low energy $\pi-\pi^*$ excitation of about 6–13 nm in MeCN, and the calculated energies are closer to those observed experimentally. The only exception are triazolo-pyridine derivatives **5** and **6** in which the $\pi-\pi^*$ excitations are slightly blue-shifted in the polar solvent.

2.3. Chelation of MgH₂

The chelating ability of the triazoles **7** was assessed by examining complexes with MgH₂ using computational methods and comparing the results to those for other related ligands. Results in Table 2 indicate that 2-substituted benzotriazoles have enthalpies of complex formation of about -22 kcal/mol, which are similar to those calculated for *bpy* (**1**) and significantly smaller than those for anions **2** and **3**. As expected, the introduction of nitrogen atoms to the azine ring diminishes the electron density at the coordinated nitrogen atom and lowers its donating abilities. Consequently, the order of the exotherm follows **7a** > **7c** > **7d** > **7b** > **7e**. The

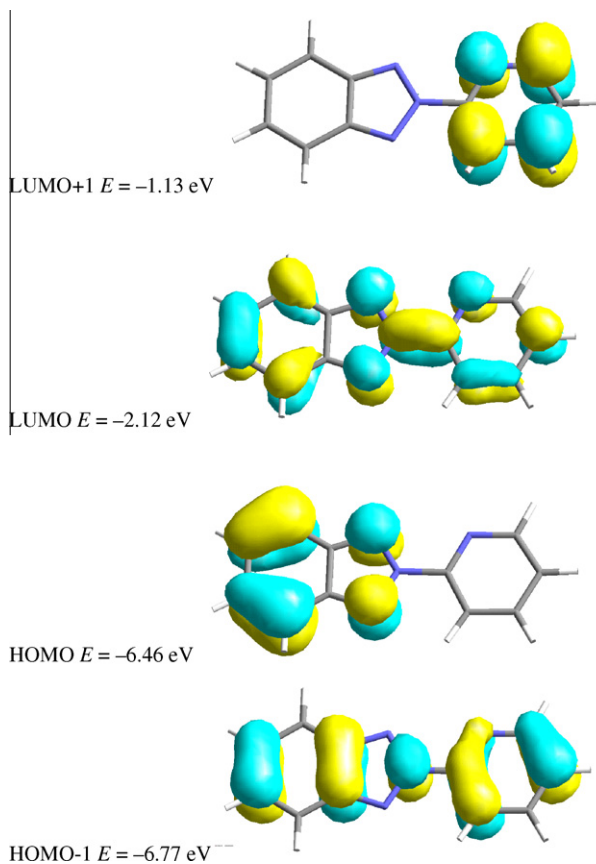


Fig. 4. B3LYP/6-311G(d, p) derived contours and energies of A'' -symmetric molecular orbitals relevant to low energy transitions in **7a**.

methoxy group in **9** increases the electron density on the ring and the coordinated nitrogen atom. As a result, the enthalpy of complex formation is larger by 0.7 kcal/mol and the electron density on the MgH_2 fragment is increased by 0.026e relative to the parent pyridazine complex **7d-Mg**. In comparison to pyridine derivative **7a**, the exotherm of complex formation for the isomeric ligand **5** is lower by about 3.3 kcal/mol, while for **4** and **6** the difference is significant and lower by as much as 10.1 kcal/mol for the latter.

The geometry of the benzotriazole complexes **7-Mg** does not vary much. Both $N \cdots Mg$ distances, d_6 and d_5 , fall in a range of 2.26–2.30 Å, which are longer than d_6 in the *bpy* complex **1-Mg** (2.24 Å) and d_5 in anions **2-Mg** and **3-Mg** (2.17 Å). The shortest d_5 distance is observed for the pyrimidine complex **7c-Mg** and the longest for the pyridazine complexes **7d-Mg** and **9-Mg**. The $N \cdots Mg$ distances in three isomeric complexes **4-Mg**, **5-Mg** and **7a-Mg** conform to the general range of 2.26–2.30 Å, while those found in **6-Mg** are outside the range presumably due to differences in ligand's geometry. The $H \cdots Mg \cdots H$ angle is about 142° and is slightly wider than that in the *bpy* complex **1-Mg** (137°) and significantly wider than that in the anionic derivatives **2-Mg** and **3-Mg** (125°).

2.4. Crystal and molecular structures for **7a-Ru**

Initially, dark-red crystals of **7a-Ru** were grown by slow evaporation of MeCN solutions. The resulting solvate contained two solvent molecules located about a local center in space group *P1* and the refinement of the structure was plagued with excessive correlations. No useful crystal structure determination could be obtained from least-squares refinement.

Recrystallization with a mixture of 2-butanone and toluene gave dark-red prisms of **7a-Ru** in space group *P1* [39]. The unit cell contains two $[C_{31}H_{24}N_8Ru]^{2+}$ dications, four $[PF_6]^-$ anions and one 2-butanone solvent, which replaced the two molecules of MeCN. The structure was not disordered, hence providing a relative chiral anchor for crystal structure refinement. Additionally, the relative positions of the fluorine atoms on the two $[PF_6]^-$ anions are distinctly non-centrosymmetric [40]. Details for the structure solution and refinement procedures are given in SI.

Both unique dications *A* and *B* have similar geometry with the Ru atoms exhibiting the normal octahedral coordination as shown for *A* in Fig. 5. The pyridine rings are practically coplanar in both 2,2'-bipyridyl (*bpy*) ligands and the dihedral angles are in a range of 0.8–3.6°. Similar coplanarity of two heterocyclic rings is observed for the benzotriazole ligand in which the dihedral angles is 2.02°(12) in *A* and 0.1°(12) in *B*.

Analysis of the bonding to Ru demonstrates that for the benzotriazole ligand the d_5 distance (2.052(5) Å in *A* (Fig. 5) and 2.048(5) Å in *B*) is shorter than the d_6 (2.089(5) Å in *A* and 2.075 Å in *B*), and similar to that found for the Ru– N_{bpy} distances (avg 2.050(5) Å in *A* and 2.062(5) Å in *B*).

The Ru $\cdots N_{triaz}$ distance d_5 observed in **7a-Ru** is longer than the analogous Ru $\cdots N_{triaz}$ separation found in **5-Ru** by nearly 0.02 Å [13]. In both complexes the Ru $\cdots N_{pyr}$ distance d_6 is longer by about 0.03 Å than that found for the 2,2'-bipyridyl ligand in **1-Ru** [41]. These experimental results followed the trend in calculated d_5 and d_6 values for magnesium complexes shown in Table 2 in which the shortest Mg $\cdots N$ distances are calculated for **1-Mg**. The bonding between Ru and 2,2'-bipyridyl, Ru $\cdots N_{bpy}$, in **7a-Ru** and **5-Ru**, remains essentially the same as in the parent complex **1-Ru** and is about 2.05 Å.

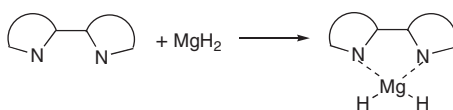
The benzotriazole ring appears to be little distorted by the coordination to the Ru center and demonstrates significant bond length alternation (bond localization) in accordance with the non-polar Kekule structure for the free ligand **7a**. The largest effect of coordination to Ru is observed for the N(2)–N(3) bond, which is longer by about 0.025 Å relative to the analogous N(4)–N(3) bond.

2.5. Characterization of **7a-Ru**

To probe the metal–ligand interactions, the ruthenium complex **7a-Ru** was characterized by spectroscopic and electrochemical methods and the results are summarized in Table 3. The complex exhibits ligand-centered absorption bands at about 300 nm and two overlapping metal-to-ligand CT bands (MLCT) in the visible range with a maximum at 434 nm (Fig. 6). Deconvoluting of the visible portion of the spectrum revealed a more intense higher energy peak with a maximum at 431 nm, and the second peak with a maximum at 473 nm [42]. The former was attributed to the Ru \rightarrow *bpy* excitation, while the low energy peak to the Ru \rightarrow **7a** excitation. This assignment is consistent with spectra of other (*bpy*)₂LRu²⁺ complexes in which the band at about 428 nm was ascribed to the Ru \rightarrow *bpy* excitation [43]. In complexes of the isomeric [1,2,3]triazole **4-Ru** and **5-Ru**, the two bands Ru \rightarrow *bpy* and Ru \rightarrow L apparently overlap giving rise to one broad absorption with a maximum at 423 nm for the former and 433 nm for the latter (Table 3). Complex **7a-Ru** exhibits a very weak emission at 690 nm ($\lambda_{ex} = 452$ nm), which by comparison to emission of **1-Ru** ($\lambda_{ex} = 452$ nm) [44] has a quantum yield of about 0.001 in EtOH at ambient temperature.

A comparison of the lowest energy MLCT bands indicates that the HOMO–LUMO separation in **7a-Ru** is smaller than that in **1-Ru** ($\lambda_{max} = 452$ nm), which in turn is smaller than that in **5-Ru** ($\lambda_{max} = 433$ nm) and in **4-Ru** ($\lambda_{max} = 423$ nm). This result is consistent with the significantly lower LUMO in **7a** free ligand (–2.12 eV, Table 1) than those in **1**, **4**, and **5** (about –1.7 eV).

Table 2
Calculated parameters for complexes of MgH₂.^a



Ligand		ΔH (kcal/mol)	d_5^b (Å)	d_6^b (Å)	q^c (e)
1		-22.4	-	2.243	-0.322
2		-47.4	2.163	2.268	-0.361
3		-48.4	2.175	2.279	-0.353
4		-14.9	2.282	2.295	-0.336
5		-20.6	2.261	2.288	-0.393
6		-13.8	2.241	2.310	-0.352
7a		-23.9	2.268	2.286	-0.430
7b		-21.7	2.272	2.300	-0.445
7c		-23.1	2.262	2.289	-0.420
7d		-22.8	2.304	2.271	-0.377
7e		-20.9	2.269	2.300	-0.418
9		-23.5	2.303	2.270	-0.403

^a B3LYP/6-31++G(d, p)//B3LYP/6-31G(d, p). With the exception of **1-Mg** (C₂) and **4-Mg** (C₁), all complexes were optimized to the C_s symmetric structures. The symmetry of ligands is given in Table 1.

^b The d_6 is the Mg distance to N atom in the 6-membered ring, and d_5 to N atom in the 5-membered ring.

^c Charge density of the MgH₂ fragment.

Cyclic voltammetry of **7a-Ru** revealed one reversible oxidation and three reversible reduction waves that are shifted to more positive potentials when compared to **1-Ru** under the same conditions.[45] The Ru²⁺/Ru³⁺ half potential for **7a-Ru** is more anodic by 0.17 V than that for **1-Ru**, which indicates lower electron donating ability of ligand **7a** when compared with 2,2'-bipyridyl (**1**). Data in Table 3 show that the weakest electron donor is **4**, 1-isomer of **7a**, as evident from the most anodic potential ($\Delta E_{1/2}^{(ox)} = +0.27$ V) of its complex **4-Ru**, while **5** is comparable to **1** ($\Delta E_{1/2}^{(ox)} = -0.03$ V).[45] The overall ligand's impact on $E_{1/2}(ox)$ of the complex appears to follow the order **5** < **1** < **7a** < **4**. The observed trend in the series does not follow the calculated charge density on the

MgH₂ fragment in complexes listed in Table 2. This is not unexpected since Mg lacks valence electron pairs and has only one ligand.

Complex **7a-Ru** is easier to reduce than **1-Ru** by +0.26 V and the reversible process at $E_{1/2}^{(red1)} = -1.00$ V is attributed to one-electron reduction of the benzo[1,2,4]triazole ligand. In contrast, the reported $E_{1/2}^{(red1)}$ potentials for complexes **4-Ru** and **5-Ru** are slightly lower than that observed for **1-Ru**. This result is consistent with the significantly lower LUMO for **7a** (-2.12 eV) than for other three free ligands (about -1.7 eV).

As a consequence of the higher reduction potential $E_{1/2}^{(red1)}$ the cell potential E_{cell} for **7a-Ru** is smaller by about 0.1 V than that

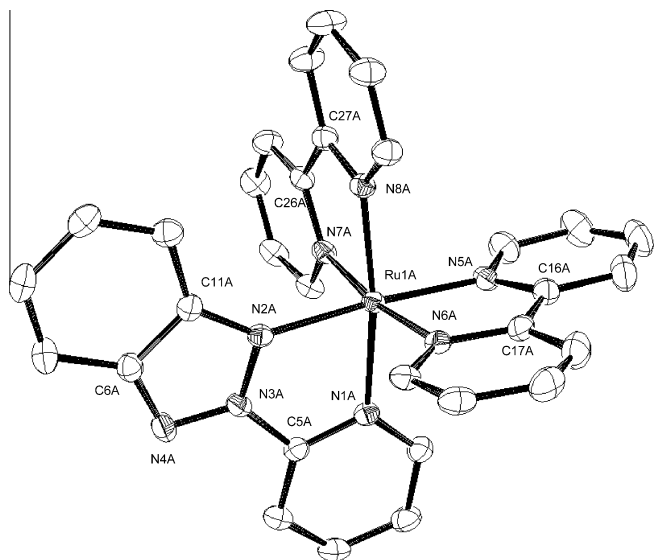


Fig. 5. Thermal ellipsoid diagram for dication **A** of **7a-Ru**. Hydrogen atoms, counterions and solvent molecule are omitted for clarity. Selected bond lengths (Å) and angles (°): Ru(1A)–N(1A) 2.089(5), Ru(1A)–N(2A) 2.052(5), Ru(1A)–N(5A) 2.052(5), Ru(1A)–N(6A) 2.067(5), Ru(1A)–N(7A) 2.035(5), Ru(1A)–N(8A) 2.047(5), N(2A)–N(3A) 1.349(7), N(3A)–N(4A) 1.320(7), C(5A)–N(3A) 1.433(7), C(16A)–C(17A) 1.458(8), C(26A)–C(27A) 1.475(7), N(2A)–C(11A) 1.348(7), N(4A)–C(6A) 1.345(7), N(2A)–Ru(1A)–N(1A) 78.6(2), N(8A)–Ru(1A)–N(7A) 78.6(2), N(5A)–Ru(1A)–N(6A) 78.8(2), N(1A)–C(5A)–N(3A)–N(2A) –2.2(12), N(5A)–C(16A)–C(17A)–N(6A) –0.8(12), N(7B)–C(26B)–C(27B)–N(8B) –2.6(13).

measured for its isomers, **4-Ru** and **5-Ru**, and **1-Ru**. This is consistent with the electronic absorption data (Table 3) and indicates the smallest HOMO–LUMO gap for **7a-Ru** in the series.

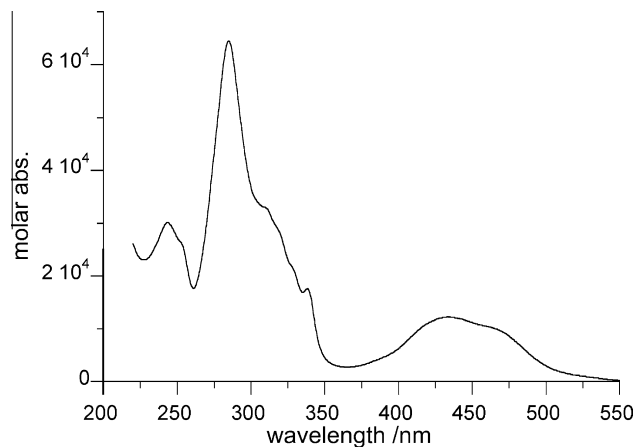


Fig. 6. Electronic absorption spectrum of **7a-Ru** recorded in MeCN.

3. Conclusions

Benzotriazoles **7** are new bidentate ligands with tunable electronic properties. A combination of experimental and computational methods allowed for extensive comparison of the triazoles to 2,2'-bipyridyl (**1**) and to their isomers **4–6** as ligands.

All benzotriazole derivatives **4–9**, **12** and **19** have lower HOMO–LUMO gaps than 2,2'-bipyridyl as evident from experimental and calculated excitation energies shown in Table 1. The lowest π – π^* excitation for benzotriazoles fall into a range of 4.16–3.91 eV (298–317 nm), which is 0.24–0.49 eV lower energy than that for **1**, although some of this difference can be due to solvent effects. 2-Substituted benzotriazoles **7** have significantly lower LUMO energies than the **1** isomers, as evident by **4** and **12**, and isomeric

Table 3
Experimental parameters for selected Ru complexes.

	A	λ_{\max} (log ϵ) ^a /nm	$E_{1/2}^{(\text{ox})\text{b}}$ /V	$E_{1/2}^{(\text{red1})\text{b}}$ /V	$E_{1/2}^{(\text{red2})\text{b}}$ /V	$E_{1/2}^{(\text{red3})\text{b}}$ /V	$E_{\text{cell}}^{\text{c}}$ /V
1-Ru		452 (4.13) ^d 450 ^e	+1.35 +1.26 ^d +1.35 ^f	–1.26 –1.33 ^d 1.33 ^f	–1.46 –1.51 ^d –1.52 ^f	<–1.70 –1.77 ^d –1.76 ^f	2.61 2.59 2.68
4-Ru		423 (4.21) ^d	+1.53 ^d	–1.39 ^d	–1.60 ^d	^g	2.92
5-Ru		433 ^e	+1.23 ^e	–1.42 ^e	–1.65 ^e	^g	2.65
7a-Ru		473 and 431	+1.52	–1.00	–1.38	–1.61	2.52

^a Low energy MLCT band recorded in MeCN.

^b Potentials vs SCE obtained in 0.1 M solution of $[\text{Bu}_4\text{N}]^+[\text{PF}_6]^-$ in MeCN vs SCE and referenced to the Fc/Fc⁺ couple assumed to be +0.46 V vs SCE [46].

^c $E_{\text{cell}} = E_{1/2}^{(\text{ox})} - E_{1/2}^{(\text{red1})}$.

^d Ref. [12].

^e Ref. [13].

^f Potentials vs SCE obtained in 0.1 M solution of $[\text{Bu}_4\text{N}]^+[\text{BF}_4]^-$ in MeCN. Ref. [47].

^g Not reported.

triazoles **4–6**. The level of the LUMO in series **7** systematically decreases for each N atom included in the aryl substituent reaching a value of -2.69 eV for the triazinyl derivative **7e**. At the same time the ligand's electron donating ability moderately diminishes. The LUMO energy of the ligands impacts the photophysical and electrochemical behavior of the complexes: the lower the ligand's LUMO the lower MLCT energy (smaller HOMO–LUMO gap) and higher reduction potential are expected. This is evident from a comparison of **7a–Ru** with their isomeric analogs **4–Ru** and **5–Ru**.

Theoretical analysis of Mg^{2+} complexes demonstrated that all 2-substituted benzotriazoles **7** have tight binding comparable to that of *bpy* (**1**) and higher than that for isomeric pyridyl derivatives **4–6**. This is supported by experimental molecular structures of Ru^{2+} complexes shown in Table 3.

Overall, new 2-aziny-2H-benzotriazoles **7** expand and complement the existing pool of bidentate ligands for designing of mono- and dinuclear metal complexes and deserve further investigation. Functional derivatives such as **8** provide a potential synthetic handle for the preparation of functional materials including surface anchoring of the complex.

4. Computational details

Quantum-mechanical calculations were carried out at the B3LYP/6-31G(d, p) and B3LYP/6-311G(d, p) level of theory using GAUSSIAN 98 and 09 suites of programs [48,49]. Geometry optimizations were undertaken using default convergence limits and with appropriate symmetry constraints. Vibrational frequencies were used to characterize the nature of the stationary points. Zero-point energy (ZPE) corrections were scaled by 0.9806 [50].

Following general recommendations [51], energy for complex formation were derived as the differences of SCF energies of individual species computed using the 6-31++G(d, p) basis set at the geometries obtained with the 6-31G(d, p) basis set (single point calculations). Thermodynamic corrections were obtained using the 6-31G(d, p) basis set.

Electronic excitation energies for the triazoles were obtained at the B3LYP/6-311G(d, p) level using the time-dependent DFT method [52] supplied in the Gaussian package. Solvent effects on electronic absorptions were requested using the SCRF(PCM, Solvent = CH₃CN) keywords.

5. Experimental section

Melting points are uncorrected. ¹H NMR spectra were recorded at 300 MHz in CDCl₃ and referenced to the solvent (7.27 ppm). The IR spectra were measured in KBr pellet. UV spectra were recorded in UV-grade CH₃CN. All compounds were in concentration of $0.6\text{--}6 \times 10^{-5}$ M. Extinction coefficients were obtained by fitting the maximum absorbance against concentration in agreement with Beer's law.

5.1. Electrochemistry

Electrochemical analysis of **1–Ru** and **7a–Ru** was conducted under dry argon in MeCN (distilled over CaH₂) containing freshly dried [Bu₄N]⁺[PF₆][−] (50 °C, P₂O₅, vacuum, overnight) as the supporting electrolyte (0.1 M) and glassy carbon working electrode with Ag/AgNO₃ (1 mM in MeCN) electrode as reference. The scanning rate was 0.1 V/s. Peak potentials were referenced to the Fc/Fc⁺ couple (+0.142 V) by adding small amounts of ferrocene to the solution, which was assumed to be +0.462 V vs SCE (MeCN, 0.1 M [Bu₄N]⁺[ClO₄][−]). [46] The electrochemical half potentials for **1–Ru** and **7a–Ru** were identical when less stringent experimental conditions were used.

[(*bpy*)₃Ru]²⁺[PF₆]₂[−] (**1–Ru**) was obtained from commercial [(*bpy*)₃Ru]²⁺2Cl[−]·6H₂O by precipitation with [NH₄]⁺[PF₆][−] and double recrystallization from a MeCN/EtOH mixture.

5.2. Preparation of benzotriazoles **7a**, **7b**, **8**, and **9**. General procedure

Appropriate 2-(*o*-halophenylazo)azine **10** (1.0 mmol), sodium azide (260 mg, 4.0 mmol), and tetrabutylammonium bromide (64 mg, 0.2 mmol) were dissolved in anhydrous DMF (1.5 ml). The reaction mixture was stirred in 120 °C for 12 h. After cooling, the reaction mixture was diluted with CH₂Cl₂, and inorganic salts were filtered off. Solvents were evaporated, and the crude product was purified by column chromatography on silica gel. Analytically pure compounds were obtained by crystallization from appropriate solvent.

5.2.1. 2-(2-Pyridinyl)-2H-benzotriazole (**7a**)

A CH₂Cl₂/hexanes mixture (9:1) was used as an eluent. Yield: 155 mg (79%); colorless crystals (cyclohexane): mp 104–105 °C; ¹H NMR (CDCl₃) δ 8.70 (d, *J* = 4.6 Hz, 1H), 8.37 (d, *J* = 8.2 Hz, 1H), 7.99–7.94 (m, 3H), 7.48–7.40 (m, 3H) ppm; IR (KBr) ν 1572, 1472, 1433, 1286 cm^{−1}; UV, λ_{\max} (log ϵ) 304 (4.38), 228 (4.25) nm; GC–MS (EI), *m/z* 196 (M⁺, 100). Anal. Calc. for C₁₁H₈N₄: C, 67.34; H, 4.11; N, 28.55. Found: C, 67.36; H, 4.12; N, 28.58%.

5.2.2. 2-(2-Pyrazinyl)-2H-benzotriazole (**7b**)

CH₂Cl₂ with increasing amounts of MeCN (0–5%) was used as an eluent. Yield: 159 mg (81%); colorless crystals (*iso*-octane/CH₂Cl₂): mp 175–176 °C; ¹H NMR (CDCl₃) δ 9.72 (s, 1H), 8.76 (d, *J* = 2.3 Hz, 1H), 8.68 (d, *J* = 1.3 Hz, 1H), 8.02–7.97 (m, 2H), 7.52–7.48 (m, 2H) ppm; IR (KBr) ν 1477, 1400, 1286, 961, 740 cm^{−1}; UV, λ_{\max} (log ϵ) 311 (4.39), 226 (4.25) nm; GC–MS (EI), *m/z* 197 (M⁺, 100). Anal. Calc. for C₁₀H₇N₅: C, 60.91; H, 3.58; N, 35.51. Found: C, 60.96; H, 3.53; N, 35.52%.

5.2.3. 2-(2-Pyrimidinyl)-2H-benzotriazole (**7c**)

2-(2-Fluorophenylazo)pyrimidine (**10c**, 202 mg, 1.0 mmol), sodium azide (65 mg, 1.0 mmol), calcium *p*-toluenesulfonate (190 mg, 0.5 mmol), and tetrabutylammonium hydrogen sulfate (19 mg, 0.056 mmol) were dissolved in anhydrous DMA (1.5 ml). The reaction mixture was stirred at 110 °C for 6 h. After cooling, the reaction mixture was diluted with CH₂Cl₂, and inorganic salts were filtered off. Solvents were evaporated under reduced pressure, and the residue was separated by column chromatography on silica gel. Using CH₂Cl₂ with increasing amounts of MeCN as eluent, benzo[1,2,3]triazole **14** was isolated as the more polar fraction (66 mg, 56% yield). The less polar fraction (54 mg, 28% yield) contained two regioisomeric products **7c** and **12** in 1:2 ratio. Further separation (preparative TLC, SiO₂, 7% MeCN in CH₂Cl₂) allowed for isolation of 2-(pyrimidin-2-yl)benzo[1,2,3]triazole (**7c**) as colorless needles (CH₂Cl₂/*iso*-octane): mp 153–154 °C; ¹H NMR (CDCl₃) δ 9.00 (d, *J* = 4.7 Hz, 2H), 8.03–7.99 (m, 2H), 7.52–7.47 (m, 3H) ppm; IR (KBr) ν 1572, 1402, 1287, 960, 819, 746 cm^{−1}; UV, λ_{\max} (log ϵ) 299 (4.37), 228 (4.36) nm. Anal. Calc. for C₁₀H₇N₅: C, 60.91; H, 3.58; N, 35.51. Found: C, 60.97; H, 3.47; N, 35.49%.

5.3. 5-Hydroxymethyl-2-(4-methyl-2-pyridinyl)-2H-benzotriazole (**8**)

CH₂Cl₂ with increasing amounts of MeCN (0–15%) was used as an eluent. Yield: 191 mg (81%); colorless crystals (hexanes/CH₂Cl₂): mp 179–180 °C; ¹H NMR (CDCl₃) δ 8.54 (d, *J* = 4.9 Hz, 1H), 8.21 (s, 1H), 7.96–7.93 (m, 2H), 7.45 (d, *J* = 8.9 Hz, 1H), 4.86 (d, *J* = 5.4 Hz, 2H), 2.53 (s, 3H) 1.90 (t, *J* = 5.8 Hz, 1H) ppm; IR (KBr) ν 3397 (OH), 1605, 1561, 1419, 1404, 1281, 1024, 970, 834 cm^{−1}; UV, λ_{\max} (log ϵ) 308 (4.40), 229 (4.30) nm. Anal. Calc.

for C₁₃H₁₂N₄O: C, 64.99; H, 5.03; N, 23.32. Found: C, 64.81; H, 5.00; N, 23.26%.

5.4. 2-(6-Methoxy-3-pyridazinyl)-2H-benzotriazole (**9**)

CH₂Cl₂ with increasing amounts of MeCN (0–15%) was used as an eluent. Yield: 76 mg (33%); colorless crystals (iso-octane/CH₂Cl₂): mp 174–175 °C; ¹H NMR (CDCl₃) δ 8.42 (d, *J* = 9.4 Hz, 1H), 8.01–7.98 (m, 2H), 7.51–7.46 (m, 2H), 7.24 (d, *J* = 9.5 Hz, 1H), 4.26 (s, 3H) ppm; IR (KBr) *ν* 3069, 1402, 1308, 1283, 1005, 748 cm⁻¹; UV, λ_{max} (log ε) 304 (4.36) 236sh (4.10), 222 (4.31) nm; GC–MS (EI) *m/z* 227 (M⁺, 100). Anal. Calc. for C₁₁H₉N₅O: C, 58.15; H, 3.99; N, 30.82. Found: C, 58.42; H, 3.95; N, 30.56%.

5.5. [(2-(2-Pyridinyl)-2H-benzotriazole)(bpy)₂Ru]²⁺[PF₆]₂⁻ (**7a-Ru**)

2-(2-Pyridinyl)-2H-benzotriazole (**7a**, 68 mg, 0.3 mmol) and (bpy)₂RuCl₂·H₂O [53] (150 mg, 0.29 mmol, ¹H NMR (DMSO-*d*₆) δ 9.96 (d, *J* = 5.37 Hz, 1H), 8.63 (d, *J* = 8.1 Hz, 1H), 8.47 (d, *J* = 7.8 Hz, 1H), 8.06 (t, *J* = 7.2 Hz, 1H), 7.76 (t, *J* = 6.2 Hz, 1H), 7.67 (t, *J* = 8.1 Hz, 1H), 7.50 (d, *J* = 5.5 Hz, 1H) 7.09 (t, *J* = 6.8 Hz, 1H) ppm) in a 3:1 mixture of EtOH–H₂O (20 ml) were refluxed for 3 h. After cooling, solvents were evaporated, and the residue was dissolved in minimum amounts of water and filtered. An aqueous solution of [NH₄]⁺[PF₆]⁻ was added, the resulting precipitation was filtered, dissolved in CH₂Cl₂, and the solution was dried (Na₂SO₄). The crude product was purified by column chromatography (Al₂O₃, CH₂Cl₂–MeOH, 9:1) to give 240 mg (92% yield) of red crystals. The product was double recrystallized by dissolving in a small amount of MeCN and overlaying with toluene: mp > 260 °C; ¹H NMR (CD₃CN) δ 8.64 (d, *J* = 8.2 Hz, 1H), 8.54–8.49 (m, 3H), 8.46 (d, *J* = 8.2 Hz, 1H), 8.25 (td, *J*₁ = 8.0 Hz, *J*₂ = 1.4 Hz, 1H), 8.17 (td, *J*₁ = 7.9 Hz, *J*₂ = 1.4 Hz, 1H), 8.11–8.00 (m, 4H), 7.90 (d, *J* = 5.6 Hz, 1H), 7.80 (d, *J* = 5.5 Hz, 1H), 7.73 (d, *J* = 5.5 Hz, 2H), 7.67 (d, *J* = 5.6 Hz, 1H), 7.60 (t, *J* = 8.0 Hz, 1H), 7.54–7.29 (m, 6H), 6.02 (d, *J* = 8.8 Hz, 1H) ppm; UV, λ_{max} (log ε) 461sh, 434 (4.10), 339 (4.25), 306sh, 285 (4.81), 243 (4.49) nm. Anal. Calc. for C₃₁H₂₄N₈RuP₂F₁₂·MeCN: C, 42.14; H, 2.89; N, 13.40. Found: C, 42.21; H, 2.74; N, 13.56%.

5.6. Preparation of 2-(2-Halophenylazo)azines **10** and **16**. A general procedure [27]

Appropriate aminoazine (2-aminopyridine, aminopyrazine, 2-aminopyrimidine, or 3-amino-6-methoxypyridazine, 4.0 mmol) was dissolved in toluene (5.0 ml) and 50% aqueous solution of NaOH (3.4 ml) and 2-halonitrobenzene (4.5 mmol) were added. The mixture was vigorously stirred with a mechanical stirrer for 25 min at 50 °C. After cooling, water was added, and the mixture was extracted with CH₂Cl₂. Extracts were dried (Na₂SO₄), and solvents were evaporated. The residue was purified by column chromatography (silica gel) using hexane with increasing amounts of CH₂Cl₂ (0–100%) as the eluent followed by crystallization from appropriate solvent.

5.6.1. 2-(2-Fluorophenylazo)pyrazine (**10b**, X = F)

Yield 59%; red crystals (hexanes): mp 107–108 °C; ¹H NMR (CDCl₃) δ 9.07 (s, 1H), 8.68 (s, 2H), 7.85 (t, *J* = 7.7 Hz, 1H), 7.57–7.50 (m, 1H), 7.32–7.20 (m, 2H) ppm. Anal. Calc. for C₁₀H₇FN₄: C, 59.40; H, 3.49; N, 27.71. Found: C, 59.48; H, 3.45; N, 27.55%.

5.6.2. 2-(2-Fluorophenylazo)pyrimidine (**10c**, X = F)

Yield 62%; red crystals (hexanes): mp 68–69 °C; ¹H NMR (CDCl₃) δ 9.00 (d, *J* = 4.8 Hz, 2H), 7.94 (t, *J* = 7.7 Hz, 1H), 7.63–7.56 (m, 1H), 7.43 (t, *J* = 4.8 Hz, 1H), 7.37–7.25 (m, 2H) ppm; ¹H NMR (CD₃CN) δ 8.95 (d, *J* = 4.8 Hz, 2H), 7.83 (td, *J*₁ = 7.7 Hz, *J*₂ = 1.6 Hz,

1H), 7.72–7.63 (m, 1H), 7.51 (t, *J* = 4.8 Hz, 1H), 7.41 (ddd, *J*₁ = 11.0 Hz, *J*₂ = 8.4 Hz, *J*₃ = 1.0 Hz, 1H), 7.34 (t, *J* = 8.0 Hz, 1H) ppm. Anal. Calc. for C₁₀H₇FN₄: C, 59.40; H, 3.49; N, 27.71. Found: C, 59.52; H, 3.50; N, 27.66%.

5.6.3. 3-(2-Fluorophenylazo)-6-methoxypyridazine (**16**)

Yield 67%; red crystals (cyclohexane/CH₂Cl₂): mp 107–108 °C; ¹H NMR (CDCl₃) δ 7.96 (d, *J* = 9.3 Hz, 1H), 7.95–7.92 (m, 1H), 7.56–7.49 (m, 1H), 7.31–7.22 (m, 2H), 7.11 (d, *J* = 9.3 Hz, 1H), 4.25 (s, 3H) ppm. Anal. Calc. for C₁₁H₉FN₄O: C, 56.90; H, 3.91; N, 24.13. Found: C, 56.77; H, 3.73; N, 24.02%.

5.7. 1-(2-Pyrimidinyl)-1H-benzotriazole (**12**) [24]

Following the general procedure, compound **12** was isolated in 56% yield (110 mg) using CH₂Cl₂ as the eluent. Colorless crystals, (iso-octane/CH₂Cl₂): mp 169–171 °C (lit. [24] 164–165 °C); ¹H NMR (CDCl₃) δ 8.97 (d, *J* = 4.7 Hz, 2H), 8.62 (d, *J* = 8.4 Hz, 1H), 8.20 (d, *J* = 8.2 Hz, 1H), 7.67 (t, *J* = 7.5 Hz, 1H), 7.51 (t, *J* = 7.8 Hz, 1H), 7.40 (t, *J* = 4.7 Hz, 1H) ppm; IR (KBr) *ν* 1569, 1461, 1430, 1293, 1054, 742 cm⁻¹; UV, λ_{max} (log ε) 298 (4.00), 257 (4.09), 236 (4.27), 227sh (4.25) nm; MS (FAB), *m/z* 198 (MH⁺, 100); HRMS, *m/z* calcd for C₁₀H₈N₅: 198.0780; found: 198.0777.

5.8. 2-(6-Keto-1-methyl-3-pyridazinyl)-2H-benzotriazole (**17**)

Obtained in 51% yield (116 mg) as the second, more polar fraction during isolation of **9**. Yellow crystals (MeOH/CH₂Cl₂): mp > 260 °C; ¹H NMR (CDCl₃) δ 8.37 (d, *J* = 9.9 Hz, 1H), 7.99–7.94 (m, 2H), 7.51–7.45 (m, 2H), 7.21 (d, *J* = 9.9 Hz, 1H), 3.97 (s, 3H) ppm; IR (KBr) *ν* 1670 (C=O), 1597, 1264, 962, 758 cm⁻¹; UV, λ_{max} (log ε) 299 (4.29), 2.34 (4.36), 227 (2.33) nm; GC–MS (EI), *m/z* 227 (M⁺, 100). Anal. Calc. for C₁₁H₉N₅O: C, 58.15; H, 3.99; N, 30.82. Found: C, 58.07; H, 3.98; N, 30.66.

Acknowledgements

We thank to Mr. Bryan Ringstrand for help with preparing single crystal of **7a-Ru** for XRD analysis. Financial support for this work was received from the Petroleum Research Funds (PRF-47243-AC4) and NSF OISE (0532040).

Appendix A. Supplementary data

CCDC 785246 contains the supplementary crystallographic data for **7a-Ru**. These data can be obtained free of charge via <http://www.ccdc.cam.ac.uk/conts/retrieving.html>, or from the Cambridge Crystallographic Data Centre, 12 Union Road, Cambridge CB2 1EZ, UK; fax: (+44) 1223-336-033; or e-mail: deposit@ccdc.cam.ac.uk. Supplementary data associated with this article can be found, in the online version, at [doi:10.1016/j.poly.2011.02.023](https://doi.org/10.1016/j.poly.2011.02.023).

References

- [1] For example: L. Spiccia, G.B. Deacon, C.M. Kepert, *Coord. Chem. Rev.* 248 (2004) 1329; C. Kaes, A. Katz, M.W. Hosseini, *Chem. Rev.* 100 (2000) 3553; J.-P. Sauvage, J.-P. Collin, J.-C. Chambron, S. Guillerez, C. Coudret, V. Balzani, F. Barigelletti, L. De Cola, L. Flamigni, *Chem. Rev.* 94 (1994) 993; A. Juris, V. Balzani, F. Barigelletti, S. Campagna, P. Belser, A. von Zelewsky, *Coord. Chem. Rev.* 84 (1988) 85.
- [2] V. Balzani, G. Bergamini, F. Marchioni, P. Ceroni, *Coord. Chem. Rev.* 250 (2006) 1254.
- [3] G.D. D'Ambruoso, D.V. McGrath, *Adv. Polym. Sci.* 214 (2008) 87.
- [4] C. Herrero, B. Lassalle-Kaiser, W. Leibl, A.W. Rutherford, A. Aukauloo, *Coord. Chem. Rev.* 252 (2008) 456.
- [5] W. Miao, *Chem. Rev.* 108 (2008) 2506.
- [6] D. Karshedt, A.T. Bell, T.D. Tilley, *Organometallics* 25 (2006) 4471.
- [7] B. Neumann, C. Kringinger, I.-P. Lorenz, *Eur. J. Inorg. Chem.* (2007) 472.

- [8] R. Uson, L.A. Oro, J.A. Cabeza, J. Organomet. Chem. 247 (1983) 105.
- [9] T. Ohno, K. Nozaki, M. Haga, Inorg. Chem. 31 (1992) 548.
- [10] S.-F. Liu, Q. Wu, H.L. Schmider, H. Aziz, N.-X. Hu, Z. Popovic, S. Wang, J. Am. Chem. Soc. 122 (2000) 3671.
- [11] Y. Chi, P.-T. Chou, Chem. Soc. Rev. 39 (2010) 638.
- [12] C. Richardson, P.J. Steel, Dalton Trans. (2003) 992.
- [13] C.M. Fitchett, F.R. Keene, C. Richardson, P.J. Steel, Inorg. Chem. Commun. 11 (2008) 595.
- [14] J. Klingele, D. Kaase, J. Hilgert, G. Steinfeld, M.H. Klingele, J. Lach, Dalton Trans. 39 (2010) 4495.
- [15] E.C. Constable, P.J. Steel, Coordin. Chem. Rev. 93 (1989) 205.
- [16] C.J. Sumbly, Aust. J. Chem. 61 (2008) 894.
- [17] C. Richardson, P.J. Steel, Inorg. Chem. Commun. 10 (2007) 884.
- [18] C. Richardson, P.J. Steel, D.M. D'Alessandro, P.C. Junk, F.R. Keene, J. Chem. Soc., Dalton Trans. (2002) 2775.
- [19] F. Wang, X.-Y. Wu, R.-M. Yu, Z.-G. Zhao, C.-Z. Lu, J. Coord. Chem. 62 (2009) 3296.
- [20] X. Meng, S. Jin, H.W. Hou, C. Du, S.W. Hg, Inorg. Chim. Acta 362 (2009) 1519.
- [21] F. Wang, X.-Y. Wu, Z.-G. Zhao, Q.-S. Zhang, Y. Xie, R. Yu, C.-Z. Lu, Inorg. Chim. Acta 363 (2010) 1320.
- [22] H. Hartmann, M. Schulze, R. Günther, J. Prakt. Chem. 332 (1990) 331.
- [23] J.T. Manka, V.C. McKenzie, P. Kaszynski, J. Org. Chem. 69 (2004) 1967.
- [24] A.R. Katritzky, A.V. Ignatchenko, H. Lang, Heterocycles 41 (1995) 131.
- [25] A.J. Hubert, H. Reimlinger, Chem. Ber. 103 (1970) 2828.
- [26] D.I. Mason, D.I. Aldous, in: R.N. Castle (Ed.), Pyridazines, Wiley & Sons, New York, 1973, pp. 59–61. and references therein.
- [27] N. Campbell, A.W. Henderson, D. Taylor, J. Chem. Soc. (1953) 1281.
- [28] A. Jankowiak, E. Obijalska, A. Pieczonka, P. Kaszynski, Tetrahedron 67 (2011) 000.
- [29] F. Krollpfeiffer, H. Pötz, A. Rosenberg, Chem. Ber. 71 (1938) 596.
- [30] O. Dann, P. Nickel, Liebigs Ann. Chem. 667 (1963) 101.
- [31] L.P. Battaglia, M. Carcelli, F. Ferraro, L. Mavilla, C. Pelizzi, G. Pelizzi, J. Chem. Soc., Dalton Trans. (1994) 2651.
- [32] L.L. Merritt Jr., E.D. Schroeder, Acta Crystallogr. 9 (1956) 801.
- [33] A minimum with the C_{2v} symmetry was found at the B3LYP/6-31(d, p) level of theory. The C_{2v} symmetric structure optimized at the B3LYP/6-311(d, p) level of theory has an imaginary frequency of -7.7 cm^{-1} .
- [34] R.M. Claramunt, D.S. Maria, E. Pinilla, M.R. Torres, J. Elguero, Molecules 12 (2007) 2201.
- [35] H. Ait-Haddou, E. Bejan, J.-C. Daran, G.G.A. Balavoine, F. Berruyer-Penaud, L. Bonazzola, H. Smaoui-Chaabouni, E. Amouyal, J. Chem. Soc., Dalton Trans. (1999) 3095.
- [36] E. Castellucci, L. Angeloni, G. Marconi, J. Phys. Chem. 94 (1990) 1740.
- [37] K. Gopalakrishnan, P.K. Bhattacharya, J. Chem. Soc., Dalton Trans. (1981) 543.
- [38] B. Abarca, R. Aucejo, R. Ballesteros, F. Blanco, E. García-España, Tetrahedron Lett. 47 (2006) 8101.
- [39] Crystal data for **7a-Ru** (CCDC No. 785246): $C_{66}H_{56}F_{24}N_{16}OP_4Ru_2$ triclinic, $P\bar{1}$, $a = 10.4469(11)\text{ \AA}$, $b = 13.5584(15)\text{ \AA}$, $c = 13.7657(15)\text{ \AA}$, $\alpha = 95.429(1)^\circ$, $\beta = 93.990(1)^\circ$, $\gamma = 110.843(1)^\circ$; $V = 1802.8(3)\text{ \AA}^3$, $Z = 1$, $T = 123(2)\text{ K}$, $\lambda = 0.71073\text{ \AA}$, $R(F^2) = 0.0353$ or $Rw(F^2) = 0.0926$ (for 15 767 independent reflections with $I > 2\sigma(I)$).
- [40] Upon reviewer's suggestion, the structure of **7a-Ru** was also solved as centrosymmetric in space group $P\bar{1}$. As expected, this created a centrosymmetric image of the solvent molecule where none existed in $P1$, and moved one of the $PF_6-PF_6^-$ ions. As a consequence, the residual electron density increased from $\pm 0.6\text{ e\AA}^{-3}$ to $\pm 1.2\text{ e\AA}^{-3}$. However, forcing the $P1$ -structure had practically no effect on the geometry of the dications and the overall R index.
- [41] M. Biner, H.-B. Bürgi, A. Ludi, C. Röhr, J. Am. Chem. Soc. 114 (1992) 5197.
- [42] For details see Appendix A: Supplementary Data.
- [43] J.A. Zampese, F.R. Keene, P.J. Steel, Dalton Trans. (2004) 4124.
- [44] A. Harriman, Chem. Commun. (1977) 777.
- [45] Results for **7a-Ru** are compared to our data for **1-Ru**, while for **4-Ru** and **5-Ru** the comparison is made with the co-reported data for **1-Ru**. The observed difference in results for **1-Ru** may be due to the electrolyte and reference.
- [46] I. Noviadri, K.N. Brown, D.S. Fleming, P.T. Gulyas, P.A. Lay, A.F. Masters, L. Phillips, J. Phys. Chem. B 103 (1999) 6713.
- [47] N.E. Tokel-Takvoryan, R.E. Hemingway, A.J. Bard, J. Am. Chem. Soc. 95 (1973) 6582.
- [48] M.J. Frisch et al., GAUSSIAN 09, Revision A.02, Gaussian Inc., Wallingford, CT, 2009.
- [49] M.J. Frisch et al., GAUSSIAN 98, Revision A.9, Gaussian Inc., Pittsburgh, PA, 1998.
- [50] A.P. Scott, L. Radom, J. Phys. Chem. 100 (1996) 16502.
- [51] T. Clark, J. Chandrasekhar, G.W. Spitznagel, P.V.R. Schleyer, J. Comput. Chem. 4 (1983) 294.
- [52] R.E. Stratmann, G.E. Scuseria, M.J. Frisch, J. Chem. Phys. 109 (1998) 8218.
- [53] J.G.C. Veinot, A.A. Farah, J. Galloro, F. Zobi, V. Bell, W.J. Pietro, Polyhedron 19 (2000) 331.